

Corrosion Behavior of TiC and (Ti,W)C-Reinforced Fe-17Mn and Fe-17Mn-3Al Austenitic Steel Matrix In Situ Composites

Ashok Kumar Srivastava¹ · Karabi Das² · Sandeep Kr. Toor³ · Koh-ichi Sugimoto⁴

Received: 8 February 2015 / Revised: 20 April 2015 / Accepted: 8 June 2015 / Published online: 8 July 2015
© Springer Science+Business Media New York and ASM International 2015

Abstract The corrosion behavior of Fe-17Mn and Fe-17Mn-3Al austenitic steel matrix composites reinforced with TiC and (Ti,W)C particles, during exposure to a 3.5% NaCl aqueous solution has been reported. The corrosion behavior of these composites has been evaluated by potentiodynamic polarization curves and linear polarization resistance measurements at a scan rate of 1 mV/s at room temperature (25 ± 2 °C). Tafel extrapolation technique has been used in calculating the corrosion current density (I_{corr}) and corrosion potential (E_{corr}). It has been observed that the corrosion resistance of the composites is less than that of their corresponding unreinforced matrix materials. The corrosion resistance increases with the addition of aluminum. The corrosion resistance of (Ti,W)C-reinforced composite is more than that of TiC-reinforced composite in the case of Fe-17Mn matrix while the same is not very different in the case of TiC and (Ti,W)C-reinforced Fe-17Mn-3Al austenitic steel matrix composites.

Keywords Steel matrix composites · TiC · (Ti,W)C · Corrosion resistance

✉ Ashok Kumar Srivastava
ashok.iitkgp@yahoo.co.uk

- ¹ Center of Excellence, Department of Metallurgical Engineering, School of Engineering, O. P. Jindal University, Raigarh 496001, India
- ² Department of Metallurgical and Materials Engineering, Indian Institute of Technology, Kharagpur 721302, India
- ³ Steel Foundry, Bokaro Steel Plant, Steel Authority of India Limited, Bokaro, India
- ⁴ Department of Mechanical Systems Engineering, Faculty of Engineering, Shinshu University, Nagano 3808553, Japan

Introduction

Metal-matrix composites (MMCs) have a number of advantages over conventional metals and alloys. Among the different types of MMCs, particulate composites have been the most popular over the last two decades due to the easy fabrication and low cost. In-corporation of ceramic particles into a metal matrix can enhance the physical and mechanical properties of the matrix. These improved properties are often achieved at the expense of a lower corrosion resistance, as the reinforcing particles introduce inhomogeneities on the surfaces exposed to aggressive environments. Several corrosion studies on aluminum alloy MMCs have been reported in the literature [1–3] and it is generally regarded that the reinforcement additions are detrimental to corrosion resistance of MMCs. Although there are some reports on the physical–mechanical properties of the carbide-reinforced iron or steel matrix composites [4–7], only limited information is available concerning the corrosion characteristics of the carbide-reinforced iron or steel matrix composites [8–10]. The attention given to its corrosion behavior has gradually increased in recent years. In the past decades, a number of non-destructive methods have been developed for the measurement of corrosion rate. Of these non-destructive methods, it has been found that electrochemical polarization method has relatively more applications worldwide [11].

The aim of the present work is to investigate the corrosion behavior of Fe-17Mn and Fe-17Mn-3Al austenitic steel matrix composites reinforced with TiC and (Ti,W)C particles in 3.5 wt% NaCl aqueous solution.

Experimental Procedure

The synthesis of the composites was carried out using a 25-kg high-frequency induction furnace (Inductotherm, India) in air by covering it with a ceramic block to prevent

Table 1 Chemical compositions of TiC and (Ti,W)C-reinforced Fe-17Mn and Fe-17Mn-3Al austenitic steel matrix composites

Materials	C	Mn	Si	Al	Cr	S	P	Ti	W
Fe-17Mn									
Fe-17Mn austenitic steel	1.16	17.15	0.43	0.23	0.38	0.022	0.031
TiC-reinforced composite	1.42	17.16	0.45	0.45	0.43	0.025	0.086	10.00	...
(Ti,W)C-reinforced composite	1.38	16.76	0.447	0.288	0.34	0.028	0.050	3.02	3.00
Fe-17Mn-3Al									
Fe-17Mn-3Al austenitic steel	1.09	16.94	0.36	3.25	0.46	0.013	0.087
TiC-reinforced composite	1.38	17.20	0.40	3.42	0.44	0.024	0.080	10.00	...
(Ti,W)C-reinforced composite	1.40	17.25	0.38	3.30	0.38	0.021	0.081	3.0	3.05

Table 2 The electrochemical parameters of TiC and (Ti,W)C-reinforced Fe-17Mn and Fe-17Mn-3Al austenitic steel matrix composites

Materials	E_{corr} (V)	$I_{\text{corr}} \times 10^{-6}$ (A/cm ²)	Corrosion rate $\times 10^{-2}$ (mm/year)	$R_p \times 10^3$ (Ω cm ²)	b_a (V/dec)	b_c (V/dec)
Fe-17Mn						
Fe-17Mn austenitic steel	-0.670	1.94	2.02	5.13	0.052	0.041
TiC-reinforced composite	-0.813	7.91	8.21	1.15	0.044	0.04
(Ti,W)C-reinforced composite	-0.762	4.16	4.17	2.17	0.046	0.038
Fe-17Mn-3Al						
Fe-17Mn-3Al austenitic steel	-0.649	1.79	1.79	7.91	0.056	0.074
TiC-reinforced composite	-0.742	3.75	3.97	3.87	0.061	0.072
(Ti,W)C-reinforced composite	-0.754	3.32	3.13	3.66	0.058	0.054

the oxidation of the melt to a certain extent. The steel scrap (0.049%C, 0.43%Mn, 0.028%Si, 0.023%P, 0.013%S, 0.003%Al, 0.035%Cr, all in wt%) and cast iron (4.5%C, 0.043%Mn, 1.05%Si, 0.175%P, 0.043%S, all in wt%) were initially heated to 1600 °C and maintained at this temperature for 15 min and then the temperature was raised to 1625 °C. The calculated amount of ferro-titanium (70% purity) and electrolytic manganese (95% purity), and ferro-tungsten and electrolytic manganese was added to the melt by the plunging method at 1625 °C for 10 vol.% TiC and (Ti,W)C-reinforced composite materials, respectively. The melt was stirred continuously with an iron rod, which was inserted into the melt through a small hole located at the center of the ceramic covering block at this temperature for 10 min followed by pouring in a metallic mold. The nominal compositions of the unreinforced matrix alloy as well as the composite materials are presented in Table 1.

A galvanostatic DC power supply (Metrohm Autolab B.V. PGSTAT 302 N) which can generate current pulses up to 10 A was used for electrochemical polarization studies. Experiments were conducted using the standard three-electrode configuration, with a platinum foil as a counter electrode, saturated calomel electrode as reference electrode, and the sample as a working electrode. The

surface of the examined specimens was about 1 cm². Specimens were immersed in 3.5% NaCl aqueous solution with a pH of ~6. Experiments were carried out at room temperature (25 ± 2 °C). In order to establish the open circuit potential (OCP) before measurements, the samples were immersed in the solution for 100 s. After obtaining a stable OCP, the measurements were carried out by polarizing the specimen from +0.5 to -0.5 V with respect to E_{corr} , at a scan rate of 1 mV per sec and at a step potential of 0.45 mV.

In corrosion test, quantitative information on corrosion currents and corrosion potentials can be extracted from the intersection of the slopes of the potentiodynamic linear polarization curves [12], using the Stern–Geary Eq. (1), as follows [13]:

$$I_{\text{corr}} = \frac{1}{2.303R_p} \left(\frac{b_a \times b_c}{b_a + b_c} \right), \quad (1)$$

where I_{corr} is the corrosion current density in amps/cm², R_p is the corrosion resistance in ohms cm², b_a and b_c are the anodic and cathodic Tafel slopes in volts/decade of current density, respectively, and $[(b_a \times b_c)/(b_a + b_c)]$ is known as the Tafel constant. The corrosion rate can be calculated by using Eq. (2):

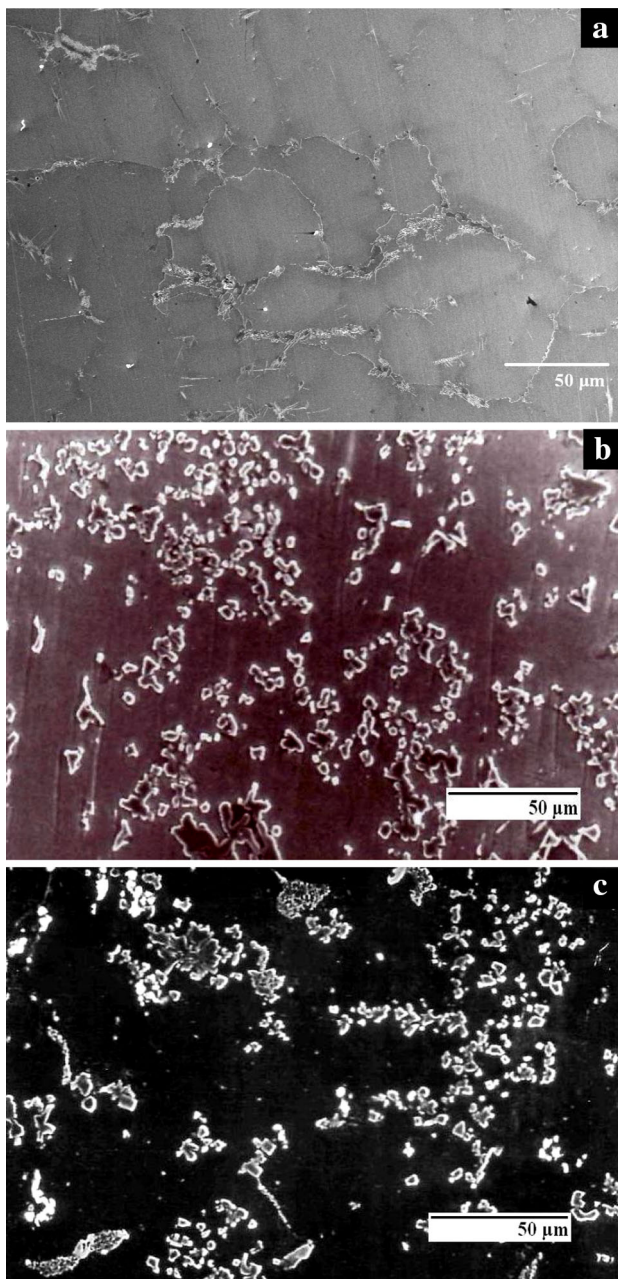


Fig. 1 SEM micrographs of **a** Fe-17Mn austenitic steel, and **b** TiC and **c** (Ti,W)C-reinforced composites

$$\text{Corrosion rate (mm/year)} = \frac{C\omega I_{\text{corr}}}{\rho}, \quad (2)$$

where C is the conversion factor, ω is the equivalent weight (g), and ρ is the density of the material (g/cm^3). The value of C has been reported as 3270, which can be calculated as $3270 = 0.01 \times [1 \text{ year (in seconds)}/96497.8]$ and $96497.8 = 1 \text{ Faraday in Coulombs}$ [14]. The corrosion potential (E_{corr}), corrosion current density (I_{corr}), corrosion rate, and polarization resistance (R_p), which have been

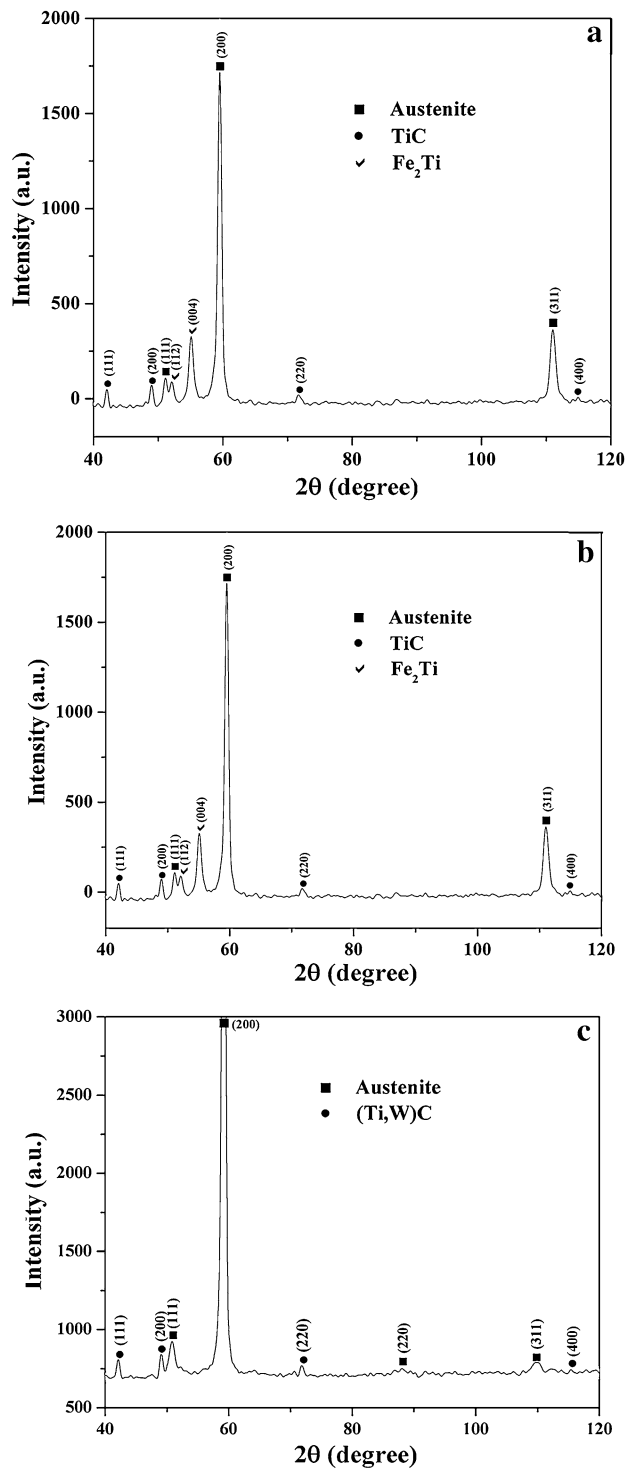


Fig. 2 XRD of **a** Fe-17Mn austenitic steel, and **b** TiC and **c** (Ti,W)C-reinforced composites

obtained from the potentiodynamic polarization curves are summarized in Table 2.

Before the potentiodynamic polarization test, the specimens were polished according to the standard

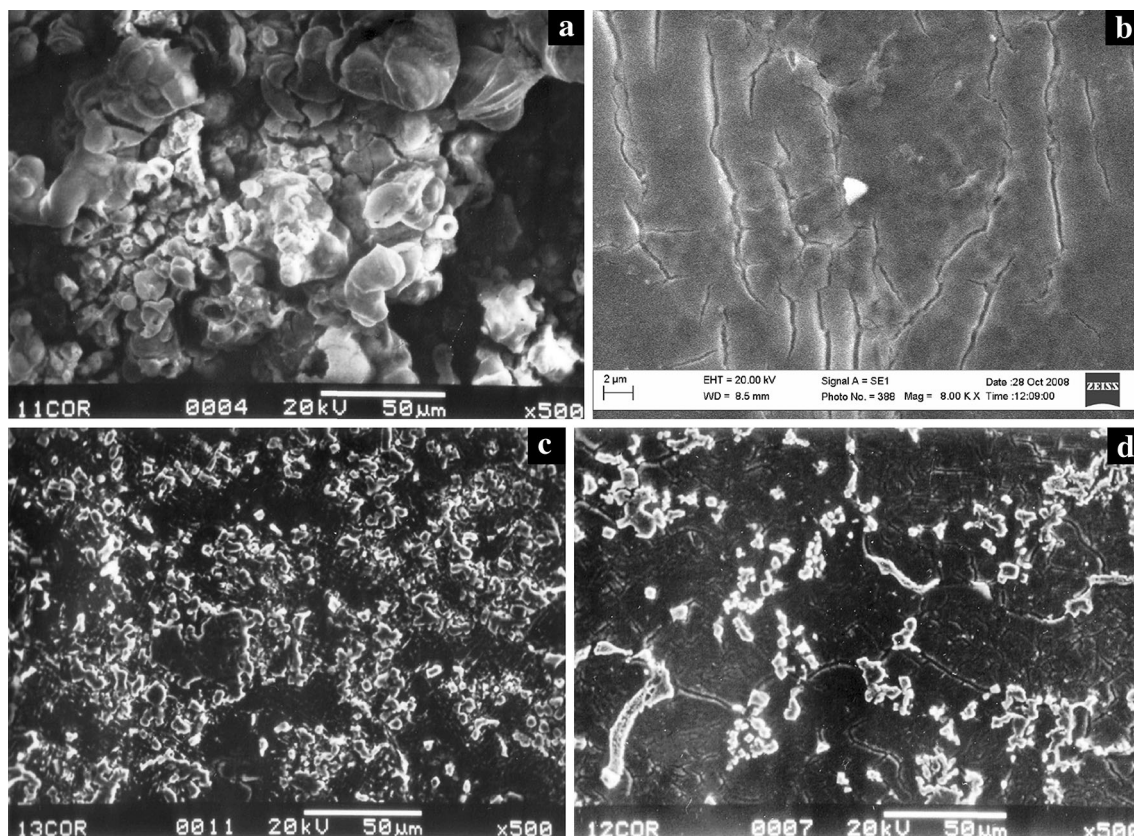


Fig. 3 SEM micrographs of corroded **a** and **b** Fe-17Mn austenitic steel, and **c** TiC and **d** (Ti,W)C-reinforced composites

metallographic technique and etched with 2% nital. The specimens were subsequently characterized using light optical microscopy (OM), scanning electron microscopy (SEM) equipped with an energy dispersive x-ray analyzer (EDS), and x-ray diffraction (XRD) analysis with CoK_α radiation. After the potentiodynamic polarization test, the samples were cleaned in acetone to remove the adhered scales and then examined using optical and scanning electron microscopy.

Results and Discussion

TiC and (Ti,W)C-Reinforced Fe-17Mn Austenitic Steel Matrix Composites

Figure 1(a) shows the SEM micrograph of as-cast Fe-17Mn austenitic steel. The microstructure consists of austenite along with very small amount of $(\text{Fe, Mn})_3\text{C}$. The SEM micrographs (Fig. 1b and c) of as-cast TiC and (Ti,W)C-reinforced composites show that the TiC and (Ti,W)C particles are distributed reasonably uniform in the matrix. The XRD patterns, shown in Fig. 2(a) to (c), confirm that the unreinforced matrix alloy is

completely austenitic and in composites, besides the austenite peaks, there are also prominent peaks of TiC and (Ti,W)C.

The SEM micrographs (Fig. 3a and b) of corroded unreinforced matrix alloy show that the localized corrosion as pitting is covered with the corrosion products and cracks are also present on the surface. These cracks may form due to drying out of the corrosion products. In case of Fe-Mn matrix, the $(\text{Fe, Mn})_3\text{C}$ carbides are precipitated along the grain boundary and embedded in a matrix of austenite, whereas in the case of Fe-Mn-Al matrix, the $(\text{Fe, Mn})_3\text{C}$ carbides and ferrite are precipitated along the grain boundary. In the case of Fe-Mn, the carbides act as cathode and the large area of austenite matrix acts as an anode which favors the pitting corrosion. In the case of Fe-Mn-Al matrix, the carbides and austenite matrix act as cathode and adjacent ferrite acts as anode which favors the pitting corrosion. It is believed that in 3.5% NaCl aqueous solution open to the air environment, pitting corrosion is distributed uniformly over the matrix and also at the austenite grains of the Fe-17Mn austenitic steel matrix alloy.

The mechanism of the pitting corrosion can be explained as that during polarization the fresh surface of the specimens exposed to oxygen containing open environment

Fig. 4 EDX spectra of the corrosion product of **a** Fe-17Mn and **b** Fe-17Mn-3Al austenitic steels

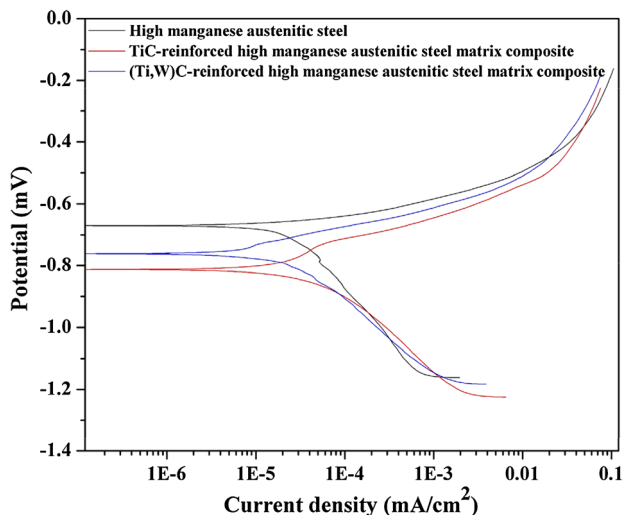
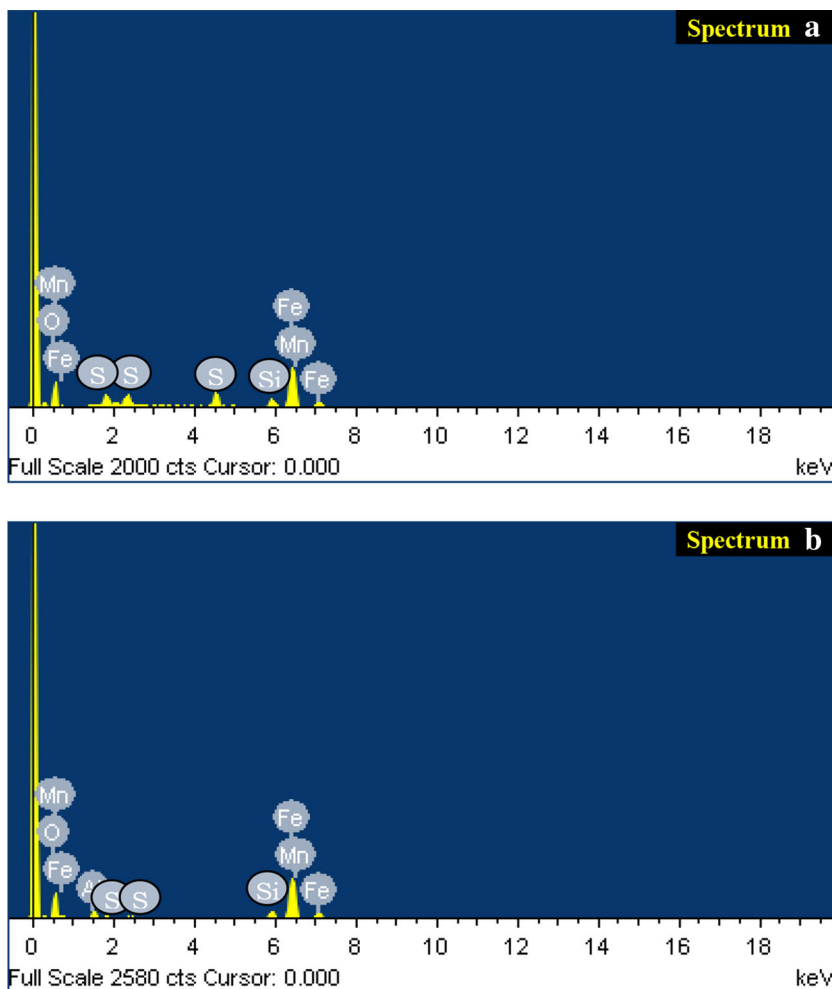


Fig. 5 Corrosion behavior of Fe-17Mn austenitic steel, and TiC and (Ti,W)C-reinforced composites

form surface oxide films (corrosion products) which are poor conductor for charge transfer. This restricts the cathodic areas to localized regions on the film which

contain defects such as phase discontinuities, second-phase precipitates, reinforcements, impurities, and microporosities [15, 16]. The initiation of pit in unreinforced matrix alloy exposed to 3.5% NaCl aqueous solution starts with the adsorption of Cl^- ions at the oxide film defects, followed by chemical reactions between the Cl^- ions and the oxide film resulting in a localized damage of the oxide film [17]. However, in composites, surface variations due to the presence of the reinforcements in the matrix can also promote film defects, and hence, the initiation of pitting is more in composites compared to that of the unreinforced matrix alloy [18, 19].

Figure 3(c) and (d) show the SEM micrographs of corroded TiC and (Ti,W)C-reinforced composites, respectively. As similar to the unreinforced matrix alloy, it can be seen that the pitting corrosion is of localized type and the surfaces are covered with the corrosion products. The EDX spectrum of Fe-Mn matrix corrosion products (Fig. 4a) shows the presence of Si and S. Sulfur, which forms MnS has a strong effect on the pitting corrosion resistance and due to which the Fe-Mn matrix is more sensitive to pitting

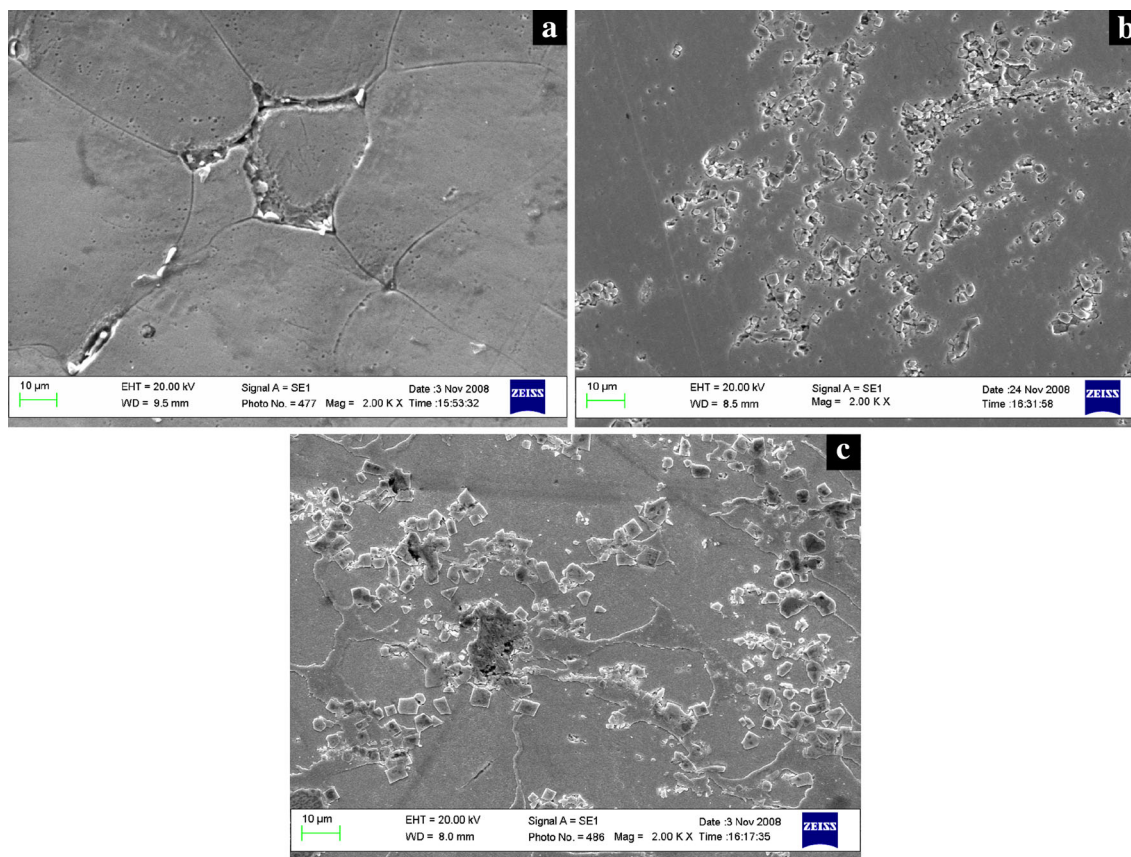


Fig. 6 SEM micrographs of **a** Fe-17Mn-3Al austenitic steel, and **b** TiC and **c** (Ti,W)C-reinforced composites

corrosion. The role of manganese sulfide inclusions on the pitting corrosion resistance has been discussed in the literature [20–23]. Manganese sulfide is harmful to the localized corrosion resistance due to its high solubility in chloride acid environments. The dissolution of this type of inclusion creates preferential sites for pit nucleation [24]. Continuous pits are observed at the particle–matrix interface suggesting an appreciable amount of corrosion at the interfacial region. It is important to note that the EDX spectrum of Fe-Mn-Al matrix corrosion products (Fig. 4b) shows very low sulfur content and, consequently, the amount of manganese sulfide inclusions is also low. Hence, the Fe-Mn-Al matrix has lesser tendency to pitting corrosion.

The severe corrosion in composites compared to unreinforced matrix alloy can be attributed to the formation of large number of local galvanic cells between austenite and noble TiC or (Ti,W)C particles which acts as a cathode during electrochemical corrosion test. It has been reported in the literature that due to the formation of interfacial film between the reinforcement and matrix or the accumulation of large dislocation density in the composites, a stress developed at the interface causes the rapid dissolution of atoms compared to their unreinforced matrix alloy and

thereby reduces the corrosion resistance of the composites compared to their unreinforced matrix alloy [25, 26].

The electrochemical parameters (E_{corr} , corrosion rate, R_p and I_{corr}) obtained from the potentiodynamic polarization curves (Fig. 5) are summarized in Table 2. It has been observed that the R_p value of the unreinforced matrix alloy is higher compared to composites and the same is higher for (Ti,W)C-reinforced composite compared to TiC-reinforced composite. Therefore, the unreinforced matrix alloy exhibits better corrosion resistance compared to composites and the (Ti,W)C-reinforced composite exhibit better corrosion resistance compared to TiC-reinforced composite. The potentiodynamic polarization curves show that the polarization behavior of all the alloys, reinforced and unreinforced, is in general quite similar. The E_{corr} value of the composites shift toward more active direction (i.e., more negative values of potential) and the values of I_{corr} and corrosion rate increases compared to unreinforced matrix alloy, which might be due to the galvanic coupling effect between the reinforcing (TiC and (Ti,W)C) particles and matrix. This behavior can be attributed to the increase in cathodic sites with the incorporation of the TiC and (Ti,W)C particles in the matrix. The smaller anodic area due to an increase in

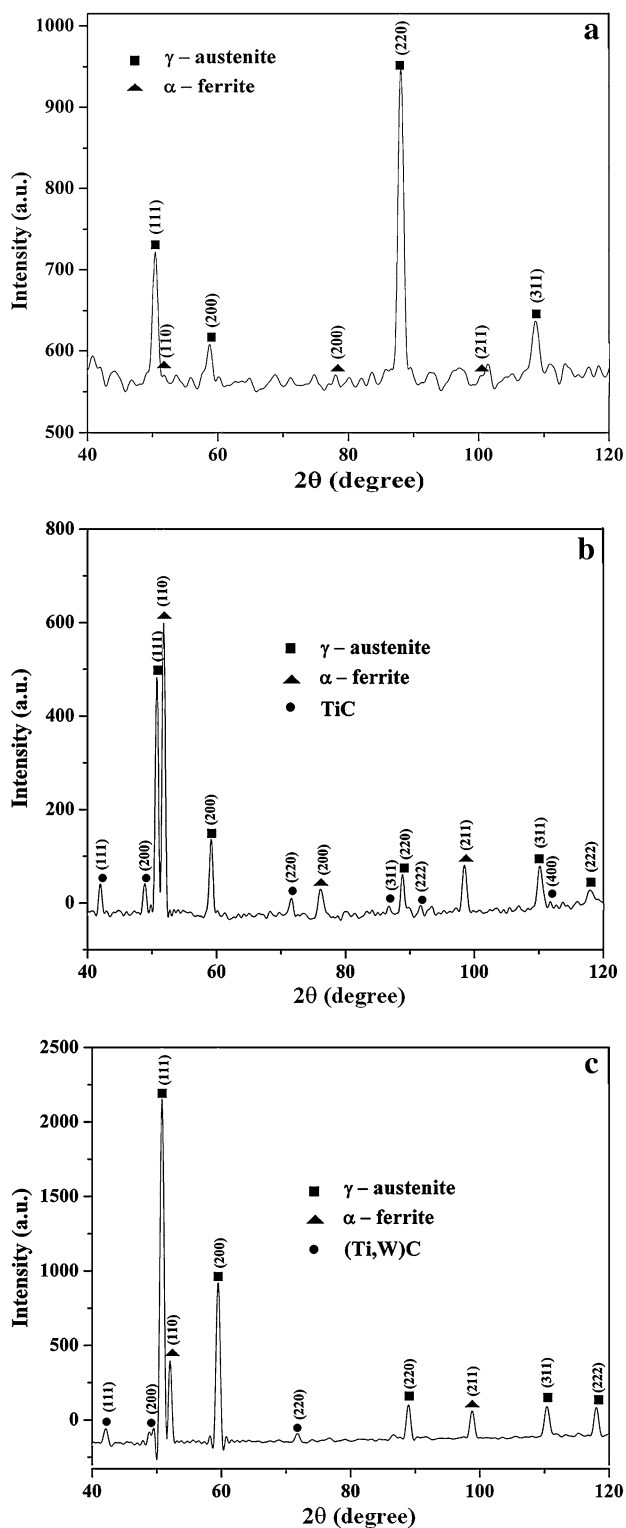


Fig. 7 XRD of **a** Fe-17Mn-3Al austenitic steel, and **b** TiC and **c** (Ti,W)C-reinforced composites

cathodic sites sustains high current density resulting in higher corrosion in composites compared to unreinforced matrix alloy.

The TiC-reinforced composite has more negative E_{corr} value and having higher values of I_{corr} and corrosion rate compared to (Ti,W)C-reinforced composite. It indicates that the TiC-reinforced composite corrode faster compared to (Ti,W)C-reinforced composite, which might be due to the following facts:

- (a) The interfaces are the preferred sites for the initiation of pitting [25, 27–29]. Diffusion of W atom in the TiC particles by substituting Ti atoms make the interface between the matrix and (Ti,W)C particles stronger than that of the same between the matrix and TiC particles. A strong interface between the (Ti,W)C particles and matrix generates less pitting and thereby increases the corrosion resistance of (Ti,W)C-reinforced composite compared to TiC-reinforced composite.
- (b) It has been reported in the literature that due to the accumulation of large dislocation density in the composite, a stress develops at the interface causing the rapid dissolution of atoms and thereby a high corrosion rate. The coefficient of thermal expansions (CTEs) of (Ti,W)C, austenitic manganese steel, and TiC are $(7.3 \times 10^{-6}/^{\circ}\text{C}$ [30]), $(1.7\text{--}2.5 \times 10^{-5}/^{\circ}\text{C}$ [31]), and $(5.5 \times 10^{-6}/^{\circ}\text{C}$ [32]), respectively. Therefore, the coefficient of thermal expansion (CTE) mismatch between the matrix and reinforcement is higher in (Ti,W)C reinforced composite compared to that in TiC reinforced composite resulting in higher corrosion rate in (Ti,W)C reinforced composite.

Therefore, it appears that the effect of interfacial area is more predominant than the effect of CTE mismatch resulting in higher corrosion resistance of (Ti,W)C-reinforced composite than that of TiC-reinforced composite.

TiC and (Ti,W)C-Reinforced Fe-17Mn-3Al Austenitic Steel Matrix Composites

Figure 6(a) shows the SEM micrograph of Fe-17Mn-3Al austenitic steel. The microstructure consists of austenite and ferrite phases. The discrete phase along the austenite grain boundary is mainly the ferrite phase. The SEM micrographs of TiC and (Ti,W)C-reinforced composites are shown in Fig. 6(b) and (c), respectively. These show the formation of TiC and (Ti,W)C particles in the matrix. The XRD and EDS analysis results are consistent with the microstructural analysis. The XRD pattern (Fig. 7a) confirms the existence of austenite and ferrite phases in unreinforced Fe-17Mn-3Al austenitic steel matrix alloy, while the XRD patterns, shown in Fig. 6(b) and (c), confirm the existence of the peaks of TiC and (Ti,W)C along with the peaks of austenite and ferrite in TiC and (Ti,W)C-reinforced composites, respectively.

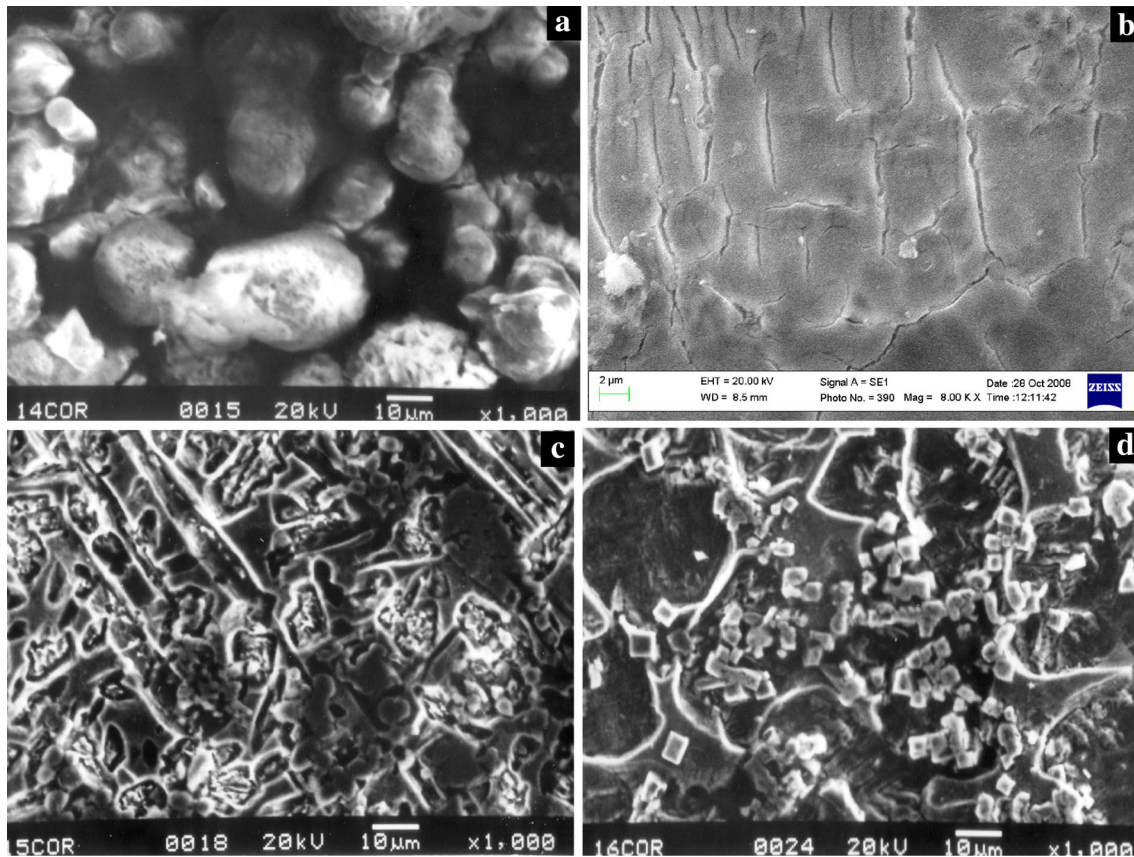


Fig. 8 SEM micrographs of corroded **a** and **b** Fe-17Mn-3Al austenitic steel at low and high magnification, respectively, and **c** TiC and **d** (Ti,W)C-reinforced composites

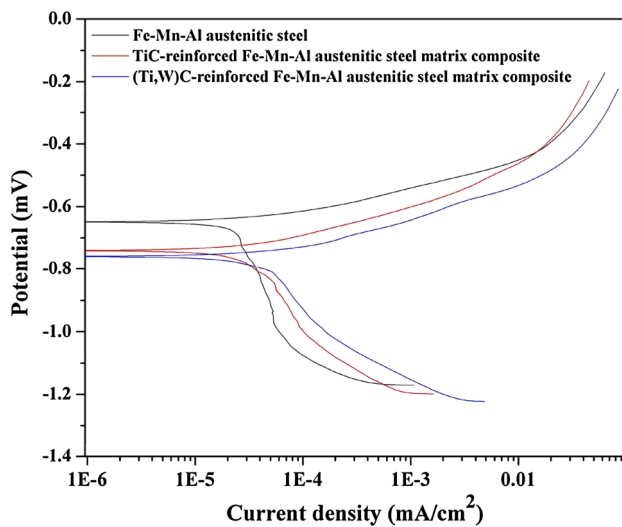


Fig. 9 Corrosion behavior of Fe-17Mn-3Al austenitic steel, and TiC and (Ti,W)C-reinforced composites

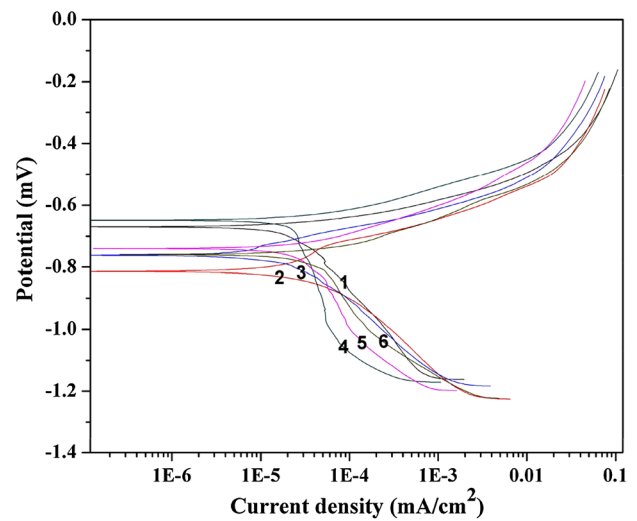


Fig. 10 Corrosion behavior of Fe-17Mn austenitic steel (1), TiC and (Ti,W)C-reinforced Fe-17Mn austenitic steel matrix composites (2 and 3), Fe-17Mn-3Al austenitic steel (4), and TiC and (Ti,W)C-reinforced Fe-17Mn-3Al austenitic steel matrix composites (5 and 6)

The SEM micrographs of corroded unreinforced matrix alloy at low and high magnification are shown in Fig. 8(a) and (b), respectively. As similar to the Fe-17Mn

austenitic steel, the area of the localized corrosion as pitting is covered with the corrosion products and having cracks on the surface. The EDX analysis (Fig. 4b) of the corrosion

products has shown the presence of the oxides of aluminum along with the oxides of iron and manganese. It can be seen from the SEM micrographs of corroded TiC and (Ti,W)C-reinforced composites that the pitting corrosion attack occurs preferentially at the interfaces of TiC particle–matrix (Fig. 8c) and (Ti,W)C-matrix (Fig. 8d), respectively. The interfacial regions may act as an effective cathode for localized corrosion on immersion in sodium chloride solution. These increase the cathode to anode ratio resulting in higher localized corrosion of the composites compared to that of the unreinforced matrix alloy. It can be seen that the TiC and (Ti,W)C-reinforced composites underwent more or less the same amount of galvanic corrosion.

The potentiodynamic polarization curves (Fig. 9) and Table 2 shows that the R_p value of the unreinforced matrix alloy is higher than that of the composites. The E_{corr} value of the composites shift toward more negative direction and the values of I_{corr} and corrosion rate increases compared to that of the unreinforced matrix alloy. The TiC and (Ti,W)C-reinforced composites have more or less the same values of E_{corr} , I_{corr} , R_p , and corrosion rate. It reveals that the unreinforced matrix alloy exhibits better corrosion resistance than that of the composites and the same of TiC and (Ti,W)C-reinforced composites are more or less the same. The composites exhibit a markedly lower corrosion resistance than their corresponding unreinforced matrix alloy can be attributed to the formation of large number of local galvanic cells between austenite and ferrite or TiC or (Ti,W)C particles which acts as a cathode during corrosion test. A film of the corrosion products which is a mixture of the oxides of iron, manganese, and aluminum forms on the surface as well as particle–matrix interface. A film of aluminum oxide is generally corrosion resistant in NaCl aqueous solution, and has poor electronic conductivity and cathode reaction ability which controls the pitting potential and rate of pitting. The corrosion resistance is imparted equally by a barrier film of the oxides of Al and Fe on the surfaces as well as particle–matrix interfaces of the TiC and (Ti,W)C-reinforced composites resulting more or less the same corrosion resistance of the TiC and (Ti,W)C-reinforced composites.

Comparison Between TiC and (Ti,W)C-Reinforced Fe-17Mn and Fe-17Mn-3Al Austenitic Steel Matrix Composites

A comparative potentiodynamic polarization curve of unreinforced and reinforced specimens of Fe-17Mn and Fe-17Mn-3Al austenitic steel is shown in Fig. 10. It can be seen from Fig. 10 and Table 2 that the values of R_p and E_{corr} of the unreinforced and reinforced specimens of Fe-17Mn-3Al austenitic steel are higher while the values of I_{corr} and corrosion rate are lower compared to the unreinforced and reinforced specimens of Fe-17Mn austenitic

steel. It reveals that the corrosion resistance of Fe-17Mn-3Al austenitic steel alloy system is better than that of the Fe-17Mn austenitic steel alloy system. This can be attributed to the fact that the standard electrode potential of aluminum (-1.66 V) is more negative than that of manganese (-1.18 V; Mn/Mn^{2+}) and the passivity coefficient of aluminum (0.82) is higher than that of manganese (0.13). With the addition of Al, the passivation ability increases which in turn increases the resistance to electrode reaction, and also a stable and compact passive protective film of aluminium oxide forms on the surface of the specimens. As a result, the corrosion resistance of Fe-17Mn-3Al matrix composite is better than that of the Fe-17Mn matrix composite.

Conclusions

In the present study, the corrosion resistance of TiC and (Ti,W)C-reinforced Fe-17Mn and Fe-17Mn-3Al austenitic steel matrix composites have been investigated. The corrosion resistance of the unreinforced matrix alloys is better than that of the composites. In the case of Fe-17Mn austenitic steel alloy system, the corrosion resistance of (Ti,W)C-reinforced is better compared to TiC-reinforced composite, while in the case of Fe-17Mn-3Al austenitic steel alloy system, the corrosion resistance of both the TiC and (Ti,W)C-reinforced composites are more or less the same.

References

1. M. Metzger, S.G. Fishman, Corrosion of aluminum-matrix composites. Status report. Ind. Eng. Chem. Prod. Res. Dev. **22**, 296–302 (1983)
2. C. Chen, F. Mansfeld, Corrosion protection of an Al 6092/SiC_p metal matrix composite. Corrosion Sci. **39**, 1075–1082 (1997)
3. S.L. Coleman, V.D. Scott, B. McEnaney, Corrosion behaviour of aluminium-based metal matrix composites. J. Mater. Sci. **29**, 2826–2834 (1994)
4. V.K. Rai, R. Srivastava, S.K. Nath, S. Ray, Wear in cast titanium carbide reinforced ferrous composites under dry sliding. Wear **231**, 265–271 (1999)
5. D. Vallauri, I.C. Atías Adrián, A. Chrysanthou, TiC-TiB₂ composites: a review of phase relationships, processing and properties. J. Eur. Cer. Soc. **28**, 1697–1713 (2008)
6. H.Y. Wang, Q.C. Jiang, B.X. Ma, Y. Wang, F. Zhao, Reactive infiltration synthesis of TiB₂-TiC particulates reinforced steel matrix composites. J. Alloys Compd. **391**, 55–59 (2005)
7. Y. Wang, Z.Q. Zhang, H.Y. Wang, B.X. Ma, Q.C. Jiang, Effects of residual F content in a sealed melting furnace on experimental results of cover gas research for magnesium alloys. Mater. Sci. Eng. A **422**, 339–345 (2006)
8. A. Trueman, D.P. Schweinsberg, G.A. Hope, The matrix corrosion of tungsten carbide/carbon steel metal matrix composites. Corrosion Sci. **39**, 1153–1164 (1997)

9. K.H. Lo, C.T. Kwok, F.T. Cheng, H.C. Man, Corrosion resistance of laser-fabricated metal-matrix composite layer on stainless steel 316L. *J. Laser Appl.* **15**, 107–114 (2003)
10. E. Pagounis, V.K. Lindroos, Processing and properties of particulate reinforced steel matrix composites. *Mater. Sci. Eng. A* **246**, 221–234 (1998)
11. Tang Luping, SP Swedish National Testing and Research Institute Building Technology SP Report (2002) 25
12. M. Debata, G.S. Upadhyaya, Corrosion behavior of powder metallurgy Y_2O_3 dispersed iron-and nickel-base superalloys. *J. Mater. Eng. Perform.* **10**, 602–607 (2001)
13. M. Stern, The mechanism of passivating-type inhibitors. *J. Electrochem. Soc.* **105**, 638–647 (1958)
14. A.C. Ciubotariu, L. Benea, M. Lakatos-Varsanyi, V. Dragan, Electrochemical impedance spectroscopy and corrosion behaviour of Al_2O_3 -Ni nano composite coatings. *Electrochem. Acta* **53**, 4557–4563 (2008)
15. G.E. Thompson, G.C. Wood, The effect of alternating voltage on aluminium electrodes in hydrochloric acid. *Corrosion Sci.* **18**, 721–746 (1978)
16. G.E. Thompson, P.E. Doherty, G.C. Wood, Observations of flaws on preconditioned aluminum surfaces. *J. Electrochem. Soc.* **129**, 1515–1517 (1982)
17. R.T. Foley, Localized corrosion of aluminum alloys—a review. *Corrosion* **42**, 277–284 (1986)
18. P.P. Trzaskoma, E. McCafferty, C.R. Crowe, Corrosion behavior of SiC/Al metal matrix composites. *J. Electrochem. Soc.* **130**, 1804–1809 (1983)
19. D.G. Kolman, D.P. Butt, Corrosion behavior of a novel SiC/ Al_2O_3 /Al composite exposed to chloride environments. *J. Electrochem. Soc.* **144**, 3785–3791 (1997)
20. P. Schmuki, H. Hildebrand, A. Friedrich, S. Virtanen, The composition of the boundary region of MnS inclusions in stainless steel and its relevance in triggering pitting corrosion. *Corros. Sci.* **47**, 1239–1250 (2005)
21. G.S. Eklund, Initiation of pitting at sulfide inclusions in stainless steel. *J. Electrochem. Soc.* **121**, 467–473 (1974)
22. D.E. Williams, R.K. Matt, C. John, G.I.N. Waterhouse, Composition changes around sulphide inclusions in stainless steels, and implications for the initiation of pitting corrosion. *Corros. Sci.* **52**, 3702–3716 (2010)
23. J. Stewart, D.E. Williams, The initiation of pitting corrosion on austenitic stainless steel: on the role and importance of sulphide inclusions. *Corros. Sci.* **33**, 457–474 (1992)
24. M.A. Baker, J.E. Castle, The initiation of pitting corrosion of stainless steels at oxide inclusions. *Corros. Sci.* **33**, 1295–1312 (1992)
25. Y. Shimizu, T. Nishimura, I. Matsushima, Corrosion resistance of Al-based metal matrix composites. *Mater. Sci. Eng.* **A198**, 113–118 (1995)
26. P.P. Trzaskoma, Pit morphology of aluminum alloy and silicon carbide/aluminum alloy metal matrix composites. *Corrosion* **46**, 402–409 (1990)
27. D. Nath, T.K.G. Namboodhiri, Some corrosion characteristics of aluminium-mica particulate composites. *Corrosion Sci.* **29**, 1215–1229 (1989)
28. H.Y. Yao, R.Z. Zhu, Interfacial preferential dissolution on silicon carbide particulate/aluminum composites. *Corrosion* **54**, 499–503 (1998)
29. H. Sun, E.Y. Koo, H.G. Wheat, Corrosion behavior of SiCp/6061 Al metal matrix composites. *Corrosion* **47**, 741–753 (1991)
30. Y. Fu, Y.W. Gu, H. Du, SiC whisker toughened Al_2O_3 -(Ti, W)C ceramic matrix composites. *Scripta Mater.* **44**, 111–116 (2001)
31. R. Castro, P. Garnier, Decomposition structures of austenitic manganese steel. *Revue de Métall.* **55**, 24–33 (1958)
32. I.E. Campbell, E.M. Sherwood (eds.), *High Temperature Materials and Technology*, vol 324 (Wiley, New York, 1967)